CrossMark

ORIGINAL PAPER

Friction and Wear Mechanism of MoS$_2$/C Composite Coatings Under Atmospheric Environment

Sheng Cai[1,2] · Peng Guo[1] · Jingzhou Liu[1] · Dong Zhang[1] · Peiling Ke[1] ·
Aiying Wang[1] · Yuejin Zhu[2]

Abstract Tribological properties of MoS$_2$/C coatings with different carbon contents (44.7–84.3 at.%) deposited by magnetron sputtering were systematically investigated under atmospheric environment. During tribological tests, the coating with the least MoS$_2$ content exhibited the lowest friction coefficient and wear rate, while coating with the most MoS$_2$ showed the worst performance. To understand friction and wear mechanism, multiple analytical tools such as SEM, EDS, Raman, XPS and TEM were applied to investigate the composition and structure. TEM and SEM characteristics proved that the tribofilm with multilayered structure was formed on the tribopair. The C-rich layer adhered to the tribopair and the top layer was well-ordered MoS$_2$ tribofilm, and the dominated amorphous MoS$_2$ was found between the two layers. It suggested that the shear plane was mainly made of well-ordered MoS$_2$ transfer film, while carbon improved the mechanical properties of the coatings, served as a lubricant and also inhibited the oxidation of MoS$_2$.

Keywords MoS$_2$ · Amorphous carbon · Mechanism · Transfer film · Re-ordering

✉ Peiling Ke
  kepl@nimte.ac.cn

✉ Aiying Wang
  aywang@nimte.ac.cn

1   Key Laboratory of Marine Materials and Related Technologies, Zhejiang Key Laboratory of Marine Materials and Protective Technologies, Ningbo Institute of Materials Technology and Engineering, Chinese Academy of Sciences, Ningbo 315201, People's Republic of China

2   Ningbo University, Ningbo 315211, People's Republic of China

1 Introduction

As solid lubricant coatings, transition metal dichalcogenides (TMDs) such as MoS$_2$ and WS$_2$ are promising candidates for applications in fields of high vacuum, aerospace, where liquid lubrication is prohibited or not available [1]. Usually, this excellent tribological behavior is due to its layered structure, which is bound by weak van der Waals forces. However, when sliding in humid air, ultra-low friction disappeared due to oxidation and unfavorable effect of water vapor [2–4]. Generally, when TMDs are used as coatings, they are porous structures and have low hardness, which would exacerbate the erosion of coatings by vapor and oxygen. As a result, the industrial application of these coatings in atmospheric environment is restricted. A widely accepted method to solve this problem is doping with other metallic elements (Ti [5, 6], Al [7], Au [8, 9], Pb [10–12], Ni [13], and Cr [14, 15]) or their compounds (ZnO [16], Sb$_2$O$_3$ [17, 18], and PbO [18, 19]), or some non-metallic elements like C [21–27], N [20, 21] to improve compactness of the coatings.

Compared with MoS$_2$ coatings doped with other elements, C-doped MoS$_2$ coatings in optimized composition and nanostructure are able to improve coatings hardness, load-bearing capacity. As a result, incorporation of C into MoS$_2$ has been one of the successful and dominant ways to achieve both good tribological and mechanical properties in humid air, which benefits from the combined excellent frictional behavior of MoS$_2$ in vacuum and dry air with the superior tribological properties of amorphous carbon (a-C) in moist air. For example, Wu et al. [24] obtained the composite coatings with outstanding hardness and elasticity by medium frequency unbalanced magnetron sputtering with (Mo + S)/C ratio from 0 to 0.19. Tribological tests in different test environments (air, N$_2$, vacuum) showed that

when (Mo + S)/C ratio was 0.12, the coatings exhibited little sensitivity to test environment. The degree of graphitization and lattice orientation of crystalline MoS_2 finally dominated the friction behavior. Coincidentally, Polcar et al. [25] reported that the hardness of MoS_2/a-C composite films (carbon content 0–55 at.%) deposited by radio frequency sputtering increased with the doped carbon content. At the same time, the composite coatings showed decreasing friction coefficients with an increasing content of carbon dry N_2 atmospheres and in humid air. Similarly, Xu et al. [26] synthesized MoS_2/a-C composite coatings by radio frequency sputtering using MoS_2 and graphite targets. Coating hardness significantly increased by increasing sputtering power from 0 to 400 W applied on graphite target, and the optimized friction performance was obtained at 300 W. The tribological results investigated by Raman spectroscopy that tribofilm released non-lubricant phases such as a-C in vacuum and MoO_3 and part of MoS_2 in ambient air indicated that the adaptive release of non-lubricant phase from tribofilm was a key issue for determining the tribological properties of MoS_2/a-C composite coatings in different sliding atmospheres. Besides, in our previous study, we synthesized MoS_2/C coatings with various carbon contents by direct current magnetron sputtering. Friction coefficient of the composite coating was quite low in ambient air and exhibited high wear resistance [28]. Though different MoS_2/C systems exhibited excellent tribological properties in atmospheric environment, the role of carbon and MoS_2 and their synergistic effect on its tribological performance are still confusing.

In this study, the tribological behaviors of MoS_2/C composite coatings with different C contents were investigated. The aim of this work is to shed light on the friction mechanism of MoS_2/C composite coatings under atmospheric environment. Thus, our main attention has been paid to analysis of the worn interfaces and wear products.

2 Experimental Details

Direct current magnetron sputtering (DCMS) system was applied for deposition of MoS_2/C coatings, as shown in detail in the previous study [28]. A graphite target with plates of pure MoS_2 (2.5 × 2.5 cm) uniformly distributed in the sputtering zone was sputtered onto mirror-finished high speed steel (HSS, for tribological test) and p-type Si (100) wafer. All substrates were cleaned ultrasonically in acetone for 20 min. Base pressure of the vacuum chamber was lower than 3×10^{-5} Torr, and the substrates were etched by Ar plasma for 20 min. The working pressure was kept at about 2.0×10^{-3} Torr by adjusting Ar flow. During deposition, the bias voltage on substrates was set at −200 V without additional heating. Ti interlayer was firstly deposited by high-power impulse magnetron sputtering using a Ti target, with the impulse parameters at 100 Hz, 200 μs, 750 V and the coupled direct current at 1.0 A. Then for MoS_2/C deposition, current of DCMS was set at 1.0 A. Carbon concentration in the coatings was controlled by changing number of MoS_2 plates stuck to a graphite target. Two and four MoS_2 plates were referred to S2 and S4, respectively, and defined S6 and S8 in the same way. Besides, pure MoS_2 and a-C coatings were deposited by using MoS_2 target and graphite target.

Tribological tests were conducted in a ball-on-disk reciprocating tribometer (Center for Tribology UMT-3), using 6-mm-diameter GCr15 (hardness-HCR60) bearing steel balls as counterparts. The reciprocating frequency was 5 Hz, and the normal load was 10 N (Corresponding Hertz contact pressure was about 0.917 GPa), producing wear tracks in length of 5 mm. The ambient temperature was around 25 °C, and relative humidity was about 35%. Thickness of as-deposited coatings and the section profile of wear tracks were measured by a surface profilometer (Alpha-Step IQ). The wear rates of tested coatings were calculated using the following equation [29]:

$$K = \frac{V}{L \times N} \tag{1}$$

where K, V, N, L represent wear rate, wear volume loss, normal load and the total sliding distance, respectively. V is calculated by plotting length and cross-sectional area of the wear tracks and takes the average by five times of measurements.

To measure the elastic modulus and hardness of the coatings, the nanoindentation system (MTS NANO G200) was applied in a continuous stiffness measurement by using a Berkovich diamond tip. Hardness and Young's modulus were determined using Oliver–Pharr analysis [30], and corresponding Poisson's ratio was 0.2. The maximum indentation depths were controlled to be 500 nm, and characteristic hardness was chosen in a depth of around 1/10 of the coating thickness to avoid the effect of substrate. Six replicate indentations were done for each sample. Atomic Force Microscopy (Veeco Dimension 3100 V) was applied to measure roughness of the selected coatings with a frame size of about 5 × 5 μm. Raman spectroscopy (Renishaw, inVia-reflex) at 532 nm wavelength was used to evaluate the bonding structure of as-deposited coatings and transfer film. Morphology of the worn surface was performed by field emission scanning electron microscope (FESEM, FEI QUANTA 250 FEG). Composition of as-deposited coatings and the worn products were analyzed by energy-dispersive X-ray spectroscopy (EDS) and multifunctional X-ray photoelectron spectroscopy (XPS, Axis ultra-DLD) using Ag Kα radiation. Focused Ion Beam (FIB) instrument (Carl Zeiss, Auriga) was applied to

prepare samples for cross-sectional transmission electron microscopy (TEM). A protective layer of Pt mixed was first deposited with the electron beam. High-resolution transmission electron microscopy (HRTEM, FEI Tecnai F20) was employed to analyze microstructure of the transfer film.

3 Results

3.1 Chemical Composition and Structure

Chemical composition, mechanical characteristics such as elastic modulus, hardness roughness and thickness of the selected coatings are shown in Table 1. EDS results included S, Mo, O and C, and the oxygen content approximately ranged from 1.01 to 3.43 at.%. Clearly, with the increasing number of MoS_2 plates, carbon concentration decreased, while S/Mo ratios fluctuated in the range of 1.45–1.70. Coatings are relatively smooth with a roughness (Ra) around 10 nm. Compared with the pure MoS_2 coatings with hardness and elastic modulus of about 1.5 and 20.1 GPa, the mechanical strength was greatly improved with elastic modulus varied from 79.7 GPa to 90.0 GPa while the hardness from 7.0 to 8.7 GPa, respectively. From S2 to S8, the coating thickness ranged from 1.2 to 1.8 μm and the interlayer for all the coatings was about 200 nm.

Since the chemical bonding and structure of these coatings were described partially in our previous works [28], the main results will be summarized here. Coating cross-sections observed by SEM showed a dense structure and TEM results showed that coatings exhibited a structure with amorphous MoS_2 embedded into amorphous carbon matrix. XPS analysis indicated only Mo–S, C=C and C–C bonds for all the coatings except for S8, which also had Mo–C bond. Raman spectroscopy confirmed the XPS and TEM results by showing the typical amorphous carbon peaks at about 1390 and 1540 cm^{-1} corresponding to D peak and G peak, respectively, as shown in Fig. 1, while the MoS_2 peak (250–500 cm^{-1}) could not be detected for
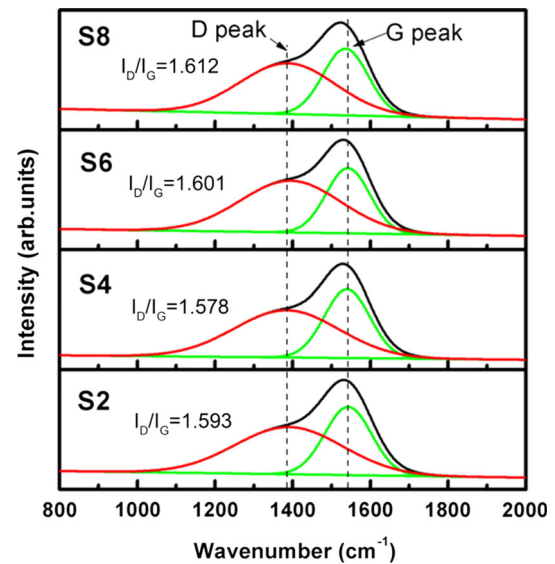

Fig. 1 Raman spectra of MoS_2/C coatings and the corresponding I_D/I_G ratio

its amorphous structure. In addition, no peaks of molybdenum oxides were detected particularly MoO_3 at the range of 800–1000 cm^{-1} [28]. This was consistent with XPS result that no Mo–O bond was found. Thus, O was not in the form of molybdenum oxides but might be dissolved in the coatings or adsorbed onto the surface. Figure 1 also shows I_D/I_G and G peak position, which can indirectly reflect the content change of sp^2 and sp^3 carbon bond atoms. It was clear that both I_D/I_G and G peak position did not change remarkably for the coatings, at about 1.6 and 1540 cm^{-1}, respectively, indicating that the carbon in all the coatings owned the similar amorphous structure [31].

3.2 Tribological Test Results

The friction curve and mean friction coefficient are shown in Fig. 2a, b, respectively. The running-in time was approximately 50 s, during which the friction coefficient declined rapidly. Within the first 10 min, the steady friction coefficient of S2 and S4 was approaching, while S8 was a

Table 1 Chemical composition and mechanical character of the coatings

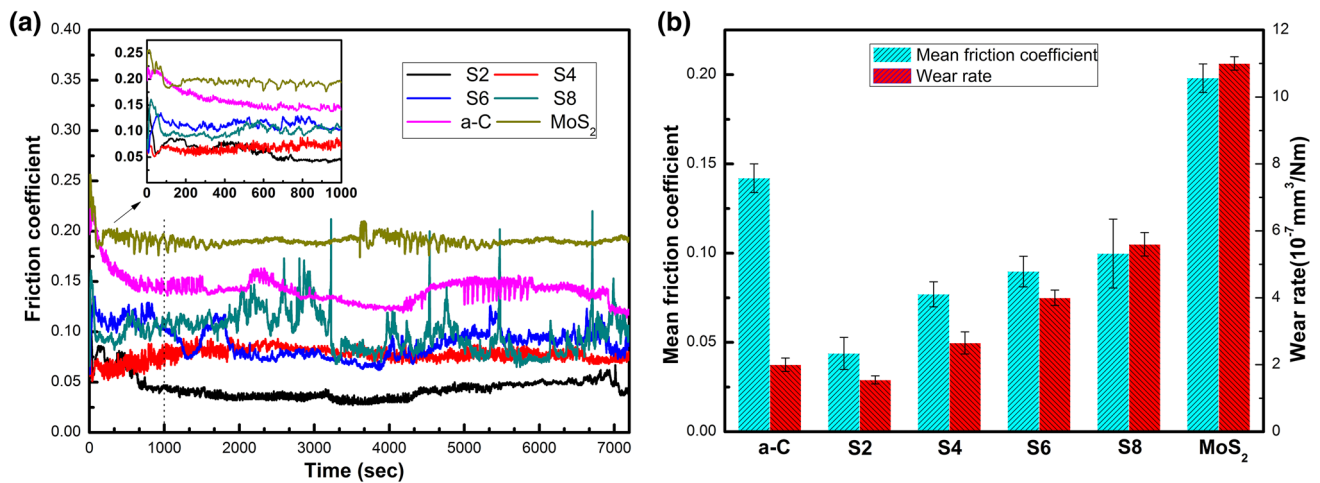| Sample	Chemical composition (at.%)				S/Mo ratio	Roughness (Ra/nm)	Elastic modulus (GPa)	Hardness (GPa)	Thickness (μm)
	C	Mo	S	O					
S2	84.33	5.54	9.12	1.01	1.65	10.5	90.0	8.7	1.2
S4	65.60	11.63	19.79	2.98	1.70	11.3	79.7	7.9	1.3
S6	55.27	15.10	26.30	3.33	1.74	9.8	85.0	7.2	1.5
S8	44.73	20.81	30.23	3.43	1.45	10.1	82.3	7.0	1.8
a-C	98.32	–	–	1.68	–	9.6	150.1	14.8	0.8
MoS_2	–	36.15	60.73	3.12	1.68	13.3	20.1	1.5	2.5

Fig. 2 Tribological results of the coatings. **a** Friction curve of the six coatings, and **b** mean friction coefficient at steady state and specific wear rate

little less than S6. The reason might be the low sliding speed, so it took a relative long time to reach the steady stage. During the steady stage, S2 stabilized with the lowest mean friction coefficient of 0.046, S4 was closed to S6 with a mean friction coefficient of 0.076 and 0.086, respectively. However, the friction curve of S8 was fluctuant and its mean friction coefficient (0.10) was the highest. For comparison, friction curve and the mean friction coefficient of the pure amorphous carbon (a-C) coating and MoS_2 coating are also shown in Fig. 2, which mean friction were 0.142 (a-C) and 0.198 (MoS_2), respectively, much higher than MoS_2/C composites. The mean wear rates are shown in Fig. 2b. The wear rates were low at the order of 10^{-7} mm^3/Nm for MoS_2/C composite

coatings and a-C coating. From S2 to S8, the wear rate increased from about 1.7 to 5.7×10^{-7} mm^3/Nm, while MoS_2 coating had the highest wear rate. In summary, the friction coefficient and the wear rates showed an upward tendency with a decreasing content of C. This tendency was different from our previous study [28], which may be caused by the different relative humidity and the normal load during the tribological test.

3.3 Worn Surface Characterization

Figure 3a shows SEM images of wear tracks. In the middle of wear tracks, flaky debris appeared due to the reciprocating friction. Many particles accumulated at the edge of
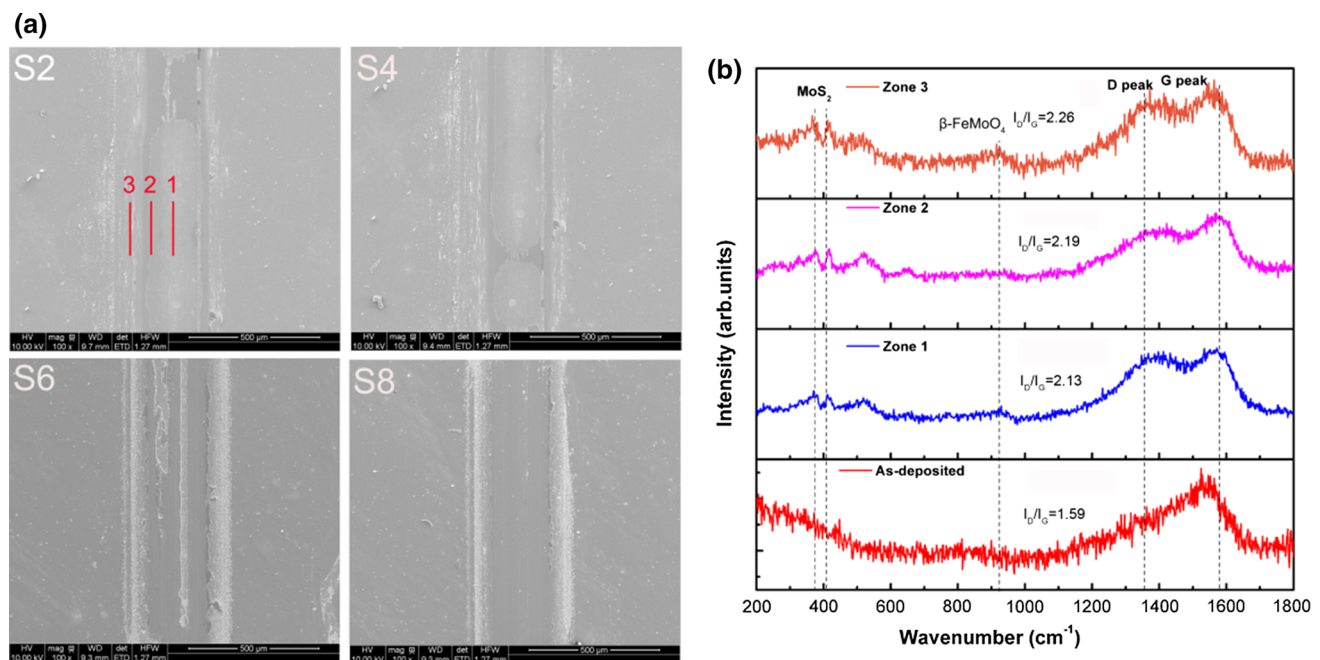

Fig. 3 a SEM images of wear tracks of the four coatings, **b** Raman spectra of the different areas of wear track of S_2
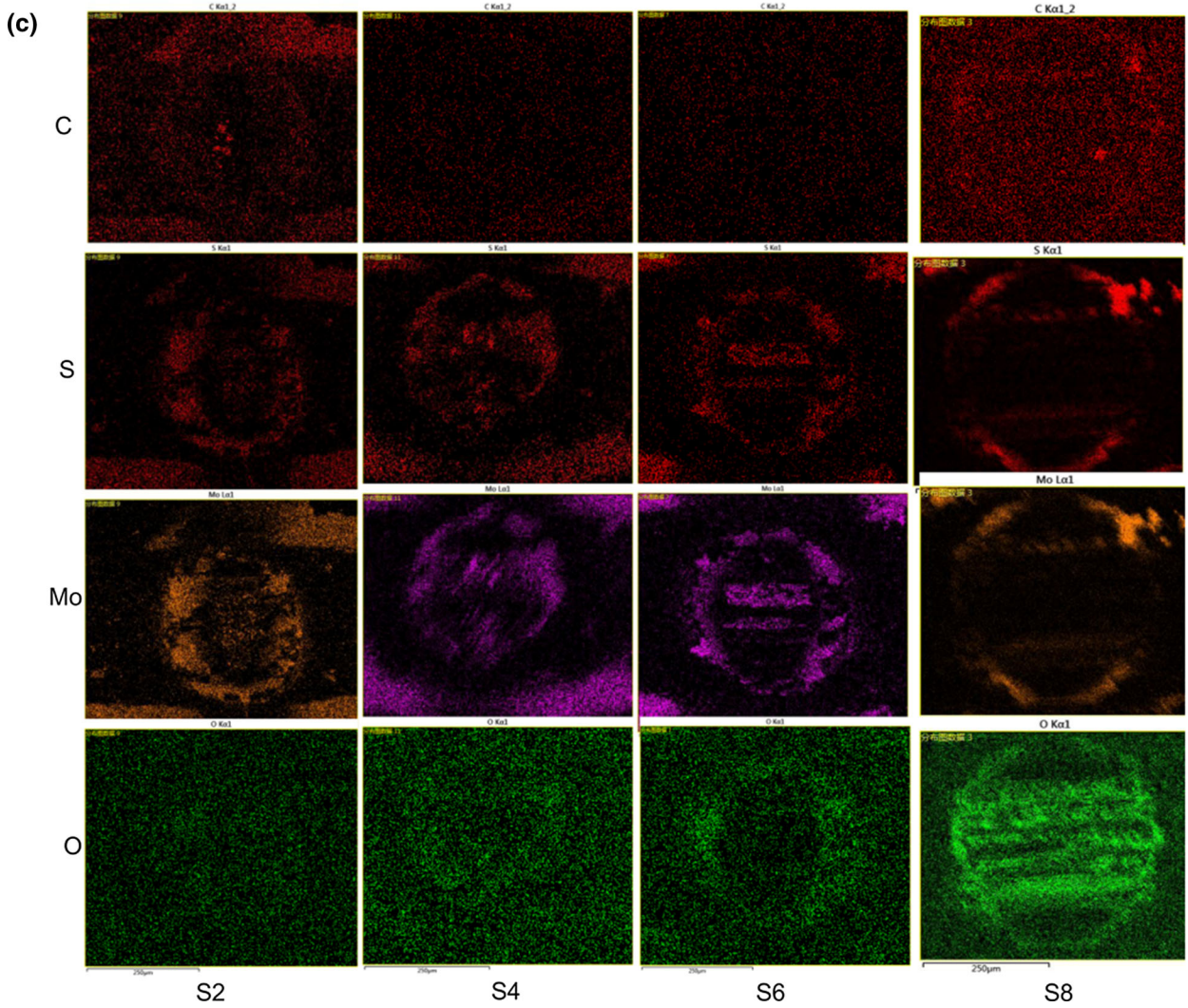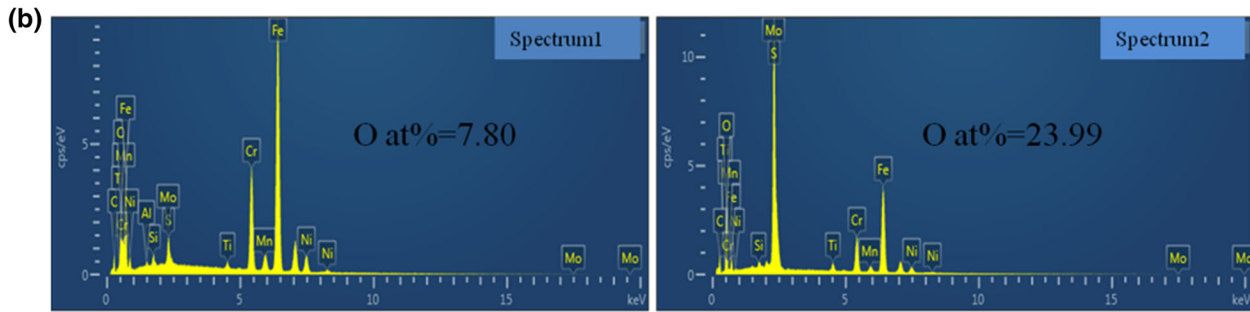
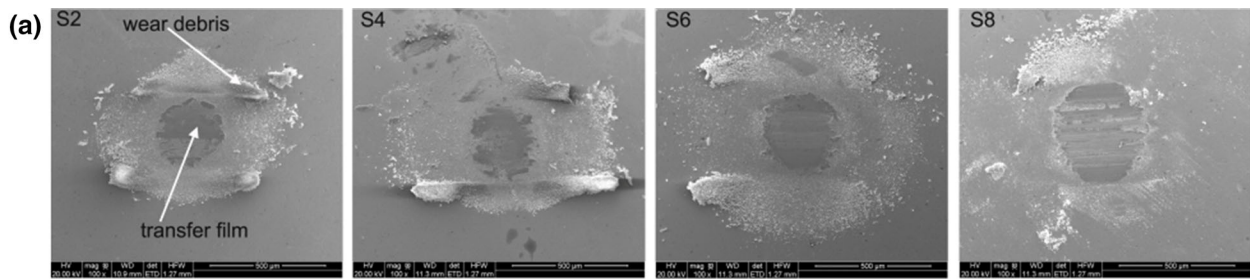**(a)** S2 wear debris, transfer film; S4; S6; S8

(b) Spectrum1 O at%=7.80; Spectrum2 O at%=23.99

(c) C; S; Mo; O — S2, S4, S6, S8

wear track, which might firstly exist in the wear track and then move to the edge. Generally, during the friction process, materials with higher shear strength tended to be thrown out from the interface, while materials with lower shear strength would remain in the interface [32]. Raman spectra taken from different areas of the wear track and the as-deposited coatings are shown in Fig. 3b. Take S2 as an example since samples showed similar results. Different from the as-deposited coatings, features within the wear track around 380, 410, 526 and 650 cm^{-1} were observed at the three different areas (identified as zone 1, 2, 3 in Fig. 3b), which were identified to be the in-plane E_{2g}, out-of-plane A_{1g}, $E_{1g} + LA$ (M) and $A_{1g} + LA$ (M) vibrations of MoS_2, respectively [33]. The peak around 930 cm^{-1} observed was usually assigned to β-$FeMoO_4$ [12], which was more obvious for zone 3, indicating that there were more Mo oxides at the edge of the wear track. Furthermore, D and G peak for amorphous carbon materials around 1360 and 1580 cm^{-1} also appeared. Specifically, compared to the as-deposited coatings, D peak of the wear track was obviously enhanced, and I_D/I_G ratio of the three zones increased greatly to 2.26, 2.19 and 2.23, respectively [31]. It was implied that rubbing these coatings in atmospheric environment induced the re-ordering of the amorphous MoS_2 and a strong graphitization of the amorphous carbon in the wear tracks.

Transfer film usually formed by the combination of direct adhesion of coating materials on the ball surface during the contact and partial sintering of wear particles for TMDs [34].Similarly, the contact areas on all balls tested here were also covered by a relatively well-adhering transfer film, as shown in Fig. 4a. It revealed that the contact area was covered with uniform transfer film which was dark in the picture, while the white wear debris distributed around; also the area of the wear scar became a little larger with the decreasing content of C atoms in the coating. In Fig. 4b, EDS showed the white wear debris contained more O element than that within the dark transfer film, suggesting that these white debris might be mainly oxides of the coating and the mating materials. Further, a remarkable signal of C, S, Mo, O elements in Fig. 4c confirmed that the main ingredient of transfer film originated from the coating. Importantly, the remarkable signal of oxygen element (Fig. 4c) increased with the decreased C content in the coatings. The oxidation of the transfer film aggravated.

In order to figure out the chemical bonds of C, S, Mo elements in the transfer films of different MoS_2/C coatings, the wear scars were further investigated by XPS, as shown in Fig. 5. Tests were done before and after 5-min etching by Ar ion beam of 2 keV, with etching depth about 20 nm. C 1s, S 2p and Mo 3d spectra of the transfer film of S2 before etching were also fitted by Guassian–Lorentian function.

C 1s spectrum was fitted into four components, where two of them represented C–C bond (285.1 eV) and C=C bond (284.6 eV), another two shoulders at approximately 288.7 and 286.5 eV corresponded to C=O and C–O, respectively [35], as shown in Fig. 5a. S 2p spectrum was fitted into three peaks, two of them represented S 2p 3/2 (163.4 eV) and S 2p 1/2 (162.1 eV) in MoS_2 structure, and the remaining represented oxide of S (168.7 eV), which could be usually assigned to SO_4^{2-} [36], as shown in Fig. 5c. For Mo 3d in Fig. 5e, the peaks representing Mo^{4+} in MoS_2 (229.2 and 232.7 eV) and peaks corresponding to Mo^{6+} in MoO_3 or β-$FeMoO_4$ (233.1 and 235.7 eV) were found, and a small shoulder (around 226.1 eV) corresponding to S 2s peak also appeared [37]. Besides, the relative content of C–O/C=O decreased, while the relative content of SO_4^{2-} increased by the calculation of integrated intensity ratio of C–O/C=O, SO_4^{2-} in percentage (Fig. 5g), suggesting that the oxidation degree of C decreased and the oxidation degree of S aggravated from S2 to S8. However, no significant difference of Mo^{6+} content was found, implying that the oxidation degree of Mo did not change greatly.

After etching, nearly no oxide peak was found in C 1 s spectra except for S2, where a weak oxide peak of C was observed, as shown in Fig. 5b. As for S8, the peak representing C–Mo (283.6 eV) was found [35], which also appeared in the as-deposited coatings for S8 but not found in the transfer film before etching. These non-lubricant metal carbides may act as hard phases to lead to the fluctuant of friction and impair the formation of wear resistant tribofilms for S8. In Fig. 5d, no oxide peak showed in all the S 2p spectra. For Mo 3d spectra, only S6 and S8 showed weak oxide peak, as shown in Fig. 5f. Consequently, with decreasing C content, the oxidation degree of S aggravated, while the oxidation degree of C was in the opposite trend, and the oxidation mainly occured on the surface of the transfer film.

TEM cross section of the transfer film on the steel ball was prepared using FIB. Figure 6 shows TEM cross section, where relatively uniform film spread on the steel ball. Figure 7a shows cross-sectional TEM image and the selected area electron diffraction (SAED) patterns of the transfer film on the steel ball surface. The area with

Fig. 5 XPS spectra of the transfer film on the ball of the four samples, and decomposition of the **a** C 1s, **c** S 2p and **e** Mo 3d spectral region of S2 before etching and **b** C 1s, **d** S 2p, **f** Mo 3d spectra after etching and **g** the relative atomic content of the C/O, S/O and Mo/O bonds of the transfer film
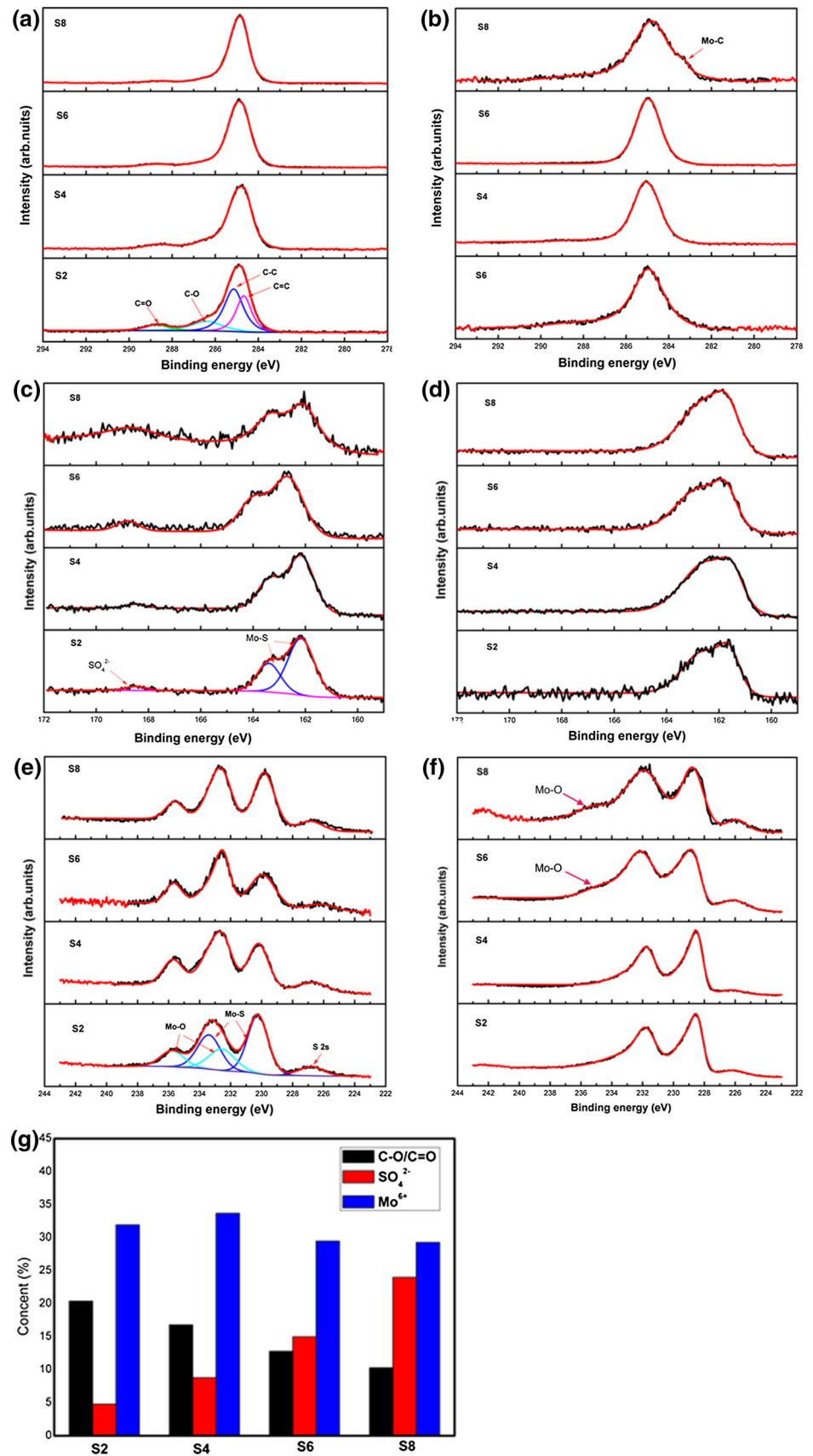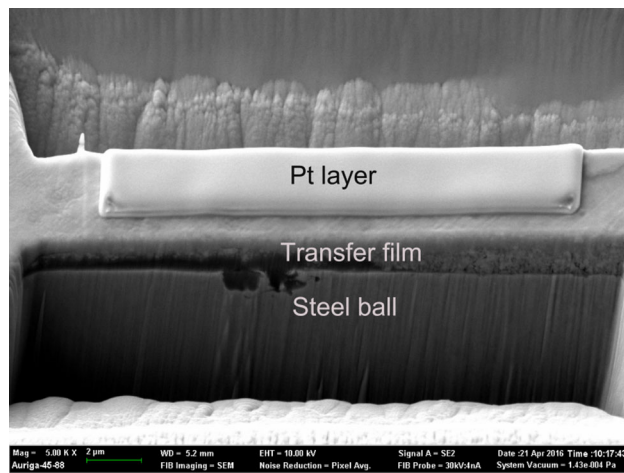
Fig. 6 SEM image of the TEM cross section of the transfer film prepared by FIB

obviously diffraction lattice was steel ball, designated as "A", and Pt layer was designated as "E". Combined with EDS and SAED results, the transfer film was consisted of an inner amorphous carbon layer (designated as "B"), an amorphous MoS_2 layer (designated as "C") and an outer crystallized MoS_2 layer (designated as "D"). In detail, "B" layer mainly contained C and a small amount of Mo, S and other mating material elements. However, "C" layer and "D" layer mainly were composed of Mo, S and trace carbon and other mating material elements. From HRTEM image shown in Fig. 7b, "B" layer possessed MoS_2 nanocrystallites existed in the amorphous carbon matrix. The typical amorphous diffraction halo in the SAED of "C" layer represented the feature of an amorphous structure. However, very few lattices were also found. Different from the other two sections of the transfer film, the topmost part was richer in MoS_2 nanocrystallites with d-spacing about 0.325 (1/2d = 0.154) nm and 0.624 (1/2d = 0.083) nm, corresponding to (004) and (002) crystal orientation, respectively, which were identified from the two faint diffraction rings shown in Fig. 7d. In this top layer, an obviously structural transformation occurred from as-deposited coating to finely aligned MoS_2 with basal plane in parallel to the shearing direction, probably due to shear stress and compressive stress. It can be speculated that the shear stress in the surface layer was stronger than the inner layer, resulting in a better crystallinity of the MoS_2.

4 Discussion

The friction coefficient and the wear rate of MoS_2/C composite coatings showed upward trend with decreasing content of C. The ex situ Raman spectra of different areas of wear track and the wear scar on the ball showed

significantly structural transformation in transferred materials, that is, a moderate graphitization of a-C phase into re-ordered graphite-like platelets and the transformation of amorphous MoS_2 into re-ordered MoS_2. This easy sheared structure was also confirmed by TEM image of the transfer film of S2 and resulted in the low friction behavior.

Specifically, in MoS_2/C composite coatings, the role of MoS_2 and carbon and the oxidation of MoS_2 were discussed here. Previous studies have reported that carbon in MoS_2/C coatings could maintain its mechanical property, thus a better tribological property of MoS_2/C than that of MoS_2 coatings [21]. In this work, MoS_2/C coatings with higher carbon content also showed lower friction coefficients and wear rates, since the much softer MoS_2 totally dominated the sliding interface during reciprocating test. Most of particular, TEM results of the transfer film corresponded to the S2 had the minimum MoS_2 content. For the other remaining three coatings, their top layer of the transfer film should also be dominated by MoS_2. In this case, interfacial shear strength should be almost the same because the interfacial layer was transformed to the easily sheared MoS_2.

The area of the wear scar became a little larger with decreased C content, suggesting the increase of real contact area. According to the equation:

$$\mu = S \times \frac{A}{N} \tag{2}$$

where μ, S, A, N is friction coefficient, shear strength, contact area and normal load, respectively. In case of the same shear strength and normal load, larger contact area will result in higher friction coefficient [38]. However, for a perfect layered MoS_2, the electronic structure leads to a net positive charge on the surface of each sheet, leading to interlayer Coulomb repulsion. Once, in presence of water molecules under atmospheric environment, the former passive sulfur layers in the layered MoS_2 will be interlocked due to hydrogen bonds, causing attractive interaction between the sheets, which could induce a higher friction coefficient [40]. At the same time, graphitization of a-C phase into re-ordered graphite-like platelets also occurred, which were prone to absorb water molecule, whose hydrogen atoms (or OH-molecules) could pacify the dangling σ bonds of the surface carbon atoms, resulting in low electron density at the surface and repulsive interaction between the adjacent graphite-like sheets [39]. The graphite-like carbon did not remain on the surface of the wear scar, but was subsequently released from the transfer film and then thrown out of the wear interface, leaving MoS_2 tribofilms along the wear scar. As a result, the top layer and interlayer of the transfer film mainly contained MoS_2 and the multilayered transfer film was formed. Comprehensively, the graphite-like sheets would protect the easy
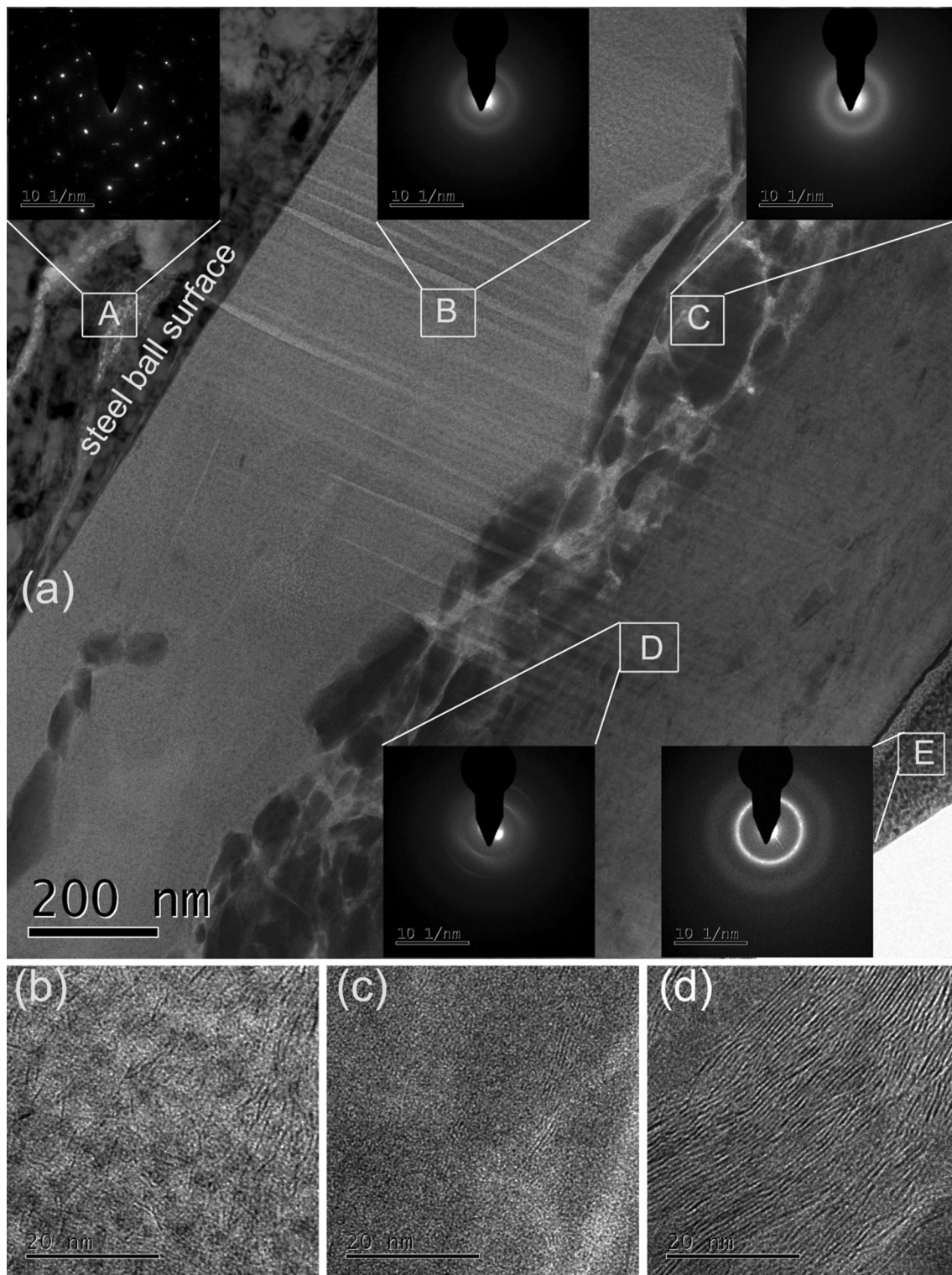
Fig. 7 **a** TEM image of the interface between the transfer film and the steel ball surface (corresponded to S_2). **b** HRTEM images of the inner carbon rich layer in transfer film marked "*B*", **c** amorphous MoS$_2$-rich layer in transfer film marked "*C*", and **d** the outer crystal MoS$_2$-rich layer in transfer film marked "*D*"

Fig. 8 A schematic representation of the friction and wearing process of MoS₂/C coating/steel ball tribopairs in atmospheric environment air
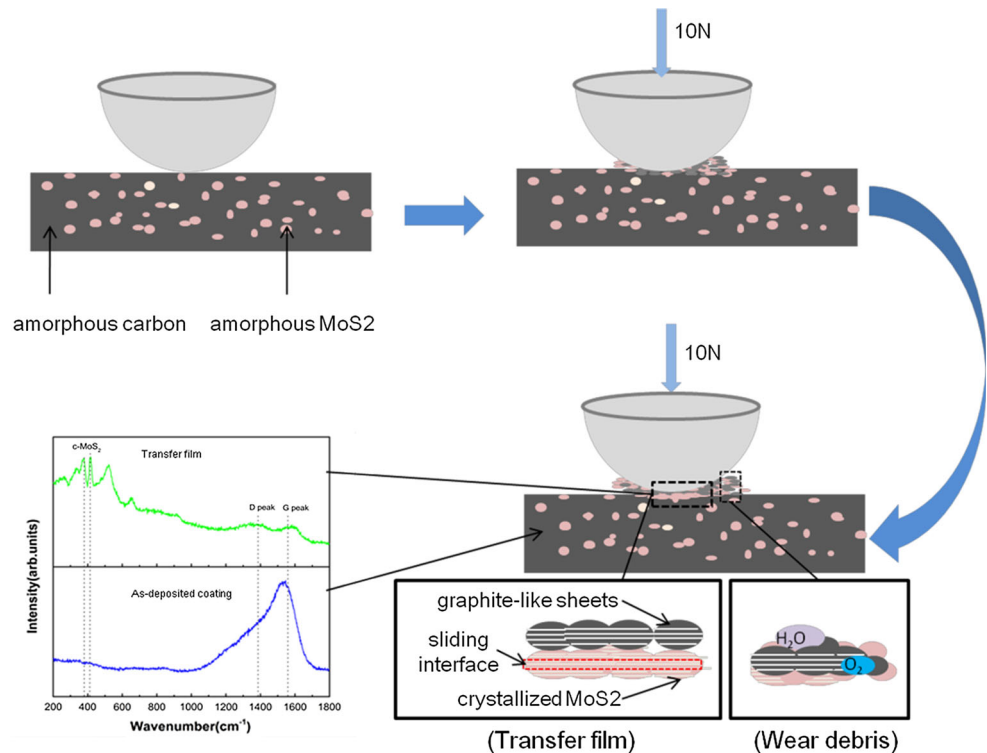
sheared MoS₂ from water erosion partially and improve tribological properties of MoS₂/C under atmospheric environment.

In addition, oxidation of MoS₂ seems to be inevitable during friction when O₂ or atomic oxygen exists. Muratore et al. [41] observed build-up of molybdenum oxide above 350 °C by in situ Raman spectroscopy that the MoS₂ was hard to be oxidized at room temperature. Even the tribological test was done at atmospheric environment about 25 °C, the oxidation of MoS₂ was difficult to occur. However, flash temperature induced by friction usually occurs in two rubbing surface, which provided energy for the oxidation of MoS₂ and C [42]. Oxidation mainly happened on the outer surface of the transfer film for the asperity, and shear stress was mainly distributed in outer surface. From the oxygen distribution map of the SEM images and XPS results, the degree of S oxidation increased with decreasing C content, which meant that C could inhibit the oxidation of MoS₂. Usually the graphitization process of amorphous carbon would consume heat generated by friction-induced annealing on the local contact areas and sliding induced strain energy [43]; thus, it would lower the oxidation of MoS₂ to some extent. However, according to the XPS results, the oxidation of Mo atom did not change significantly, which was inconsistent with the upward trend of oxidation of S when the coating had less C. From this perspective, if the degree of S oxidation increased with decreasing C content, while Mo did not change greatly, the S/Mo ratio in the MoS$_x$ phase of the

transfer film will decrease from S2 to S8, which was accounted for the high friction when the coating had less C content. Even though the S/Mo ratio of S8 in as-deposited coating was quite low, the S/Mo ratio of other three samples was quite close. For S8, the low S/Mo ratio of as-deposited coating and the severe oxidation of S element might lead to lower S/Mo ratio. Together with hard phase of Mo–C, leading to bad friction and wear behavior of S8.

Based on the results mentioned above, the possible friction and wearing process of studied MoS₂/C coatings/steel ball tribopairs sliding in atmospheric environment is deduced as illustrated in Fig. 8. Coating materials such as amorphous carbon and amorphous MoS₂ were firstly removed by the shear stress and adhered on the ball surface. In fact, the remove of coating material did not mean a truly wear, because these removed materials would transform into tribofilm between the ball and the wear track, which was responsible for the easy shear structure. During the reciprocating sliding, MoS₂ and C were partially oxidized with most of these oxide particles thrown out of the interface, then wear really occurred with material consumption. At the same time, the initially unordered structure became rearranged and resulted in a longer range ordering, which followed by eventually a crystalline structure with finely aligned MoS₂ basal plane in parallel to the shearing direction on the top layer of the transfer film. In other hand, graphitization of amorphous carbon also occurred. Consequently, the layered MoS₂ remained on the top layer of the transfer film, but most of the less-easily

sheared graphite-like sheets were thrown out of the interface, which can work as lubricants and getter of oxygen and water [27]. As a result, the sensitivity of the MoS$_2$/C composite coatings to water vapor and oxygen in humid atmospheric environment was greatly reduced.

5 Conclusions

MoS$_2$/C coatings with various C contents deposited by direct-current magnetron sputtering were tribologically evaluated against bear steel balls (GCr-15) under atmospheric environment. A low and stable friction coefficient was found for the designed coatings. Moreover, lower friction coefficients and wear rates were achieved for the coating with higher C content. Extensive analysis of worn surfaces indicated that during sliding, the relatively disordered structure became more ordered, resulting in the presence of well aligned MoS$_2$ in the interface, which was prone to shear the basal plane oriented along the sliding direction. Meanwhile, a strong graphitization of the amorphous carbon occurred in the sliding interface, where these graphite-like sheets reduced the adverse effects of moisture and oxygen on MoS$_2$. As a result, excellent lubrication performance achieved with the synergetic action of MoS$_2$ and C. The results revealed the friction and wear mechanism of MoS$_2$/C composite coatings under atmospheric environment and clearly demonstrated that the MoS$_2$/C-based coatings showed great potential for unlubricated tribological application in ordinary humid air.

References

1. Donnet, C., Erdemir, A.: Solid lubricant coatings: recent developments and future trends. Tribol. Lett. **17**, 389–397 (2004)
2. Fleischauer, P.D., Lince, J.R.: A comparison of oxidation and oxygen substitution in MoS$_2$ solid film lubricants. Tribol. Int. **32**, 627–636 (1999)
3. Khare, H.S., Burris, D.L.: Surface and subsurface contributions of oxidation and moisture to room temperature friction of molybdenum disulfide. Tribol. Lett. **53**, 329–336 (2014)
4. Zhao, X.Y., Perry, S.S.: The role of water in modifying friction within MoS$_2$ sliding interfaces. ACS Appl. Mater. Interfaces **2**, 1444–1448 (2010)
5. Renevier, N.M., Fox, V.C., Teer, D.G., Hampshire, J.: Coating characteristics and tribological properties of sputter-deposited MoS$_2$/metal composite coatings deposited by closed field unbalanced magnetron sputter ion plating. Surf. Coat. Technol. **127**, 24–37 (2000)
6. Renevier, N.M., Hamphire, J., Fox, V.C., Witts, J., Allen, T., Teer, D.G.: Advantages of using self-lubricating, hard, wear-resistant MoS$_2$-based coatings. Surf. Coat. Technol. **142–144**, 67–77 (2001)
7. Holbery, J.D., Pflüger, E., Savan, A., et al.: Alloying MoS$_2$ with Al and Au: structure and tribological performance. Surf. Coat. Technol. **169–170**, 716–720 (2003)
8. Mikhailov, S., Savan, A., Pflüger, E., et al.: Morphology and tribological properties of metal (oxide)–MoS$_2$ nanostructured multilayer coatings. Surf. Coat. Technol. **105**, 175–183 (1998)
9. Lince, J.R.: Tribology of co-sputtered nanocomposite Au/MoS$_2$ solid lubricant films over a wide contact stress range. Tribol. Lett. **17**, 419–428 (2004)
10. Wahl, K.J., Seitzman, L.E., Bolster, R.N., Singer, I.L.: Low-friction, high-endurance, ion-beam-deposited Pb–Mo–S coatings. Surf. Coat. Technol. **73**, 152–159 (1995)
11. Wahl, K.J., Dunn, D.N., Singer, I.L.: Wear behavior of Pb–Mo–S solid lubricating coatings. Wear **230**, 175–183 (1999)
12. Li, H., Zhang, G., Wang, L.: Low humidity-sensitivity of MoS$_2$/Pb nanocomposite coatings. Wear **350–351**, 1–9 (2016)
13. Lince, J.R., Hilton, M.R., Bommannavar, A.S.: Metal incorporation in sputter-deposited MoS$_2$ films studied by extended X-ray absorption fine structure. J. Mater. Res. **10**, 2091–2101 (1995)
14. Hilton, M.R., Jayaram, G., Marks, L.D.: Microstructure of cosputter-deposited metal- and oxide-MoS$_2$ solid lubricant thin films. J. Mater. Res. **13**, 1022–1029 (1998)
15. Su, Y.L., Kao, W.H.: Tribological behaviour and wear mechanism of MoS$_2$–Cr coatings sliding against various counterbody. Tribol. Int. **38**, 11–23 (2003)
16. Simmonds, M.C., Savan, A., Pfluger, E., Van Swygenhoven, H.: Mechanical and tribological performance of MoS$_2$ co-sputtered composites. Surf. Coat. Technol. **126**, 15–24 (2000)
17. Prasad, S.V., McDevitt, N.T., Zabinski, J.S.: Tribology of tungsten disulfide–nanocrystalline zinc oxide adaptive lubricant films from ambient to 500 °C. Wear **237**, 186–196 (2000)
18. Zabinski, J.S., Donley, M.S., McDevitt, N.T.: Mechanistic study of the synergism between Sb$_2$O$_3$ and MoS$_2$ lubricant systems-using Raman- spectroscopy. Wear **165**, 103–108 (1993)
19. Zabinski, J.S., Donley, M.S., Walck, S.D., Schneider, T.R., McDevitt, N.T.: The effects of dopants on the chemistry and tribology of sputter-deposited MoS$_2$ films. Tribol. Trans. **38**, 894–904 (1995)
20. Zabinski, J.S., Donley, M.S., Dyhouse, V.J., McDevitt, N.T.: Chemical and tribological characterization of PbO–MoS$_2$ films grown by pulsed laser deposition. Thin Solid Films **214**, 156–163 (1992)
21. Polcar, T., Cavaleiro, A.: Review on self-lubricant transition metal dichalcogenide nanocomposite coatings alloyed with carbon. Surf. Coat. Technol. **206**, 686–695 (2011)
22. Evaristoa, M., Nossab, A., Cavaleiro, A.: W–S–C sputtered films: influence of the carbon alloying method on the mechanical properties. Surf. Coat. Technol. **200**, 1076–1079 (2005)
23. Nossa, A., Cavaleiro, A., Carvalho, N.J.M., Kooi, B.J., De Hosson, JThM: On the microstructure of tungsten disulfide films alloyed with carbon and nitrogen. Thin Solid Films **484**, 389–395 (2005)
24. Wu, Y., Li, H., Ji, L., Ye, Y., Chen, J., Zhou, H.: Preparation and properties of MoS$_2$/a-C films for space tribology. J. Phys. D Appl. Phys. **46**, 425301 (9 pp) (2013)
25. Pimentel, J.V., Polcar, T., Cavaleiro, A.: Structural, mechanical and tribological properties of Mo–S–C solid lubricant coating. Surf. Coat. Technol. **205**, 3274–3279 (2011)
26. Xu, J., Chai, L., Qiao, L., He, T., Wang, P.: Influence of C dopant on the structure, mechanical and tribological properties of r.f.-sputtered MoS$_2$/a-C composite films. Appl. Surf. Sci. **364**, 249–256 (2016)
27. Gustavsson, F., Jacobson, S., Cavaleiro, A., Polcar, T.: Frictional behavior of self-adaptive nanostructural Mo–Se–C coatings in different sliding conditions. Wear **303**, 286–296 (2013)

28. Gu, L., Ke, P., Zou, Y., Li, X., Wang, A.: Amorphous self-lubricant MoS₂–C sputtered coating with high hardness. Appl. Surf. Sci. **331**, 66–71 (2015)

29. Kosarieh, S., Morina, A., Flemming, J., Lainé, E., Neville, A.: Wear mechanisms of hydrogenated DLC in oils containing MoDTC. Tribol. Lett. **64**, 4–21 (2016)

30. Oliver, W.C., Pharr, G.M.: An improved technique for determining hardness and elastic modulus using load and displacement sensing indentation experiments. J. Mater. Res. **7**, 1564–1583 (1992)

31. Ferrari, A.C., Robertson, J.: Interpretation of Raman spectra of disordered and amorphous carbon. Phys. Rev. B **61**, 14095–14107 (2000)

32. Stoyanov, Pantcho, Stemmer, Priska, Jarvi, Tommi T.: Friction and wear mechanisms of tungsten–carbon systems: a comparison of dry and lubricated conditions. ACS Appl. Mater. Interfaces **5**, 6123–6135 (2013)

33. Gołasa, K., Grzeszczyk, M., Leszczynski, P., Faugeras, C., Nicolet, A.A.L., Wysmołek, A., Potemski, M., Babinski, A.: Multiphonon resonant Raman scattering in MoS₂. Appl. Phys. Lett. **104**, 092–106 (2014)

34. Fusaro, R.L.: Effect of substrate surface finish on the lubrication and failure mechanisms of molybdenum disulfide films. ASLE Trans. **25**, 1–149 (1982)

35. Ji, L., Li, H., Zhao, F., Quan, W., Chen, J., Zhou, H.: Atomic oxygen resistant behaviors of Mo/diamond-like carbon nanocomposite lubricating films. Appl. Surf. Sci. **255**, 4180–4184 (2009)

36. Bernede, J.C.: About the preferential sputtering of chalcogen from transition metal dichalcogenide compounds and the determination of compound stoichiometry from XPS peak positions. Appl. Surf. Sci. **171**, 15–20 (2001)

37. Baker, M.A., Gilmore, R., Lenardi, C., Gissler, W.: XPS investigation of preferential sputtering of S from MoS₂ and determination of MoS$_x$ stoichiometry from Mo and S peak positions. Appl. Surf. Sci. **150**, 255–262 (1999)

38. Singer, I.L., Bolster, R.N., Wegand, J., Fayeulle, S., Stupp, B.C.: Hertzian stress contribution to low friction behavior of thin MoS₂ coatings. Appl. Phys. Lett. **57**, 995–997 (1990)

39. Al Mahmud, K.A.H., Kalam, M.A., Masjuki, H.H., Mobarak, H.M., Zulkifli, N.W.M.: An updated overview of diamond-like carbon coating in tribology. Crit. Rev. Solid State **40**, 90–118 (2015)

40. Gardos, M.N.: The synergistic effects of graphite on the friction and wear of MoS₂ films in air. Tribol. Trans. **31**, 214–227 (1988)

41. Muratore, C., Bultman, J.E., Aouadi, S.M., Voevodin, A.A.: Muratore. In situ Raman spectroscopy for examination of high temperature tribological processes. Wear **270**, 140–145 (2011)

42. Abdel-Aal, H.A.: A remark on the flash temperature theory. Int. Commun. Heat Mass **24**(2), 241–250 (1997)

43. Liu, Y., Erdemir, A., Meletis, E.I.: A study of the wear mechanism of diamond-like carbon films. Surf. Coat. Technol. **82**, 48–56 (1996)